

# Image acceleration in parallel magnetic resonance imaging by means of metamaterial magnetoinductive lenses

Manuel J. Freire<sup>1</sup>, Marcos A. Lopez<sup>1</sup>, Jose M. Algarin<sup>1</sup>, Felix Breuer<sup>2</sup>, and Ricardo Marqués<sup>1</sup>

<sup>1</sup>*Department of Electronics and Electromagnetism,*

*Faculty of Physics, University of Seville,*

*Avda. Reina Mercedes s/n, 41012 Sevilla, Spain \* and*

<sup>2</sup>*Research Center Magnetic Resonance Bavaria (MRB), Würzburg, Germany*

(Dated: February 19, 2022)

## Abstract

Parallel magnetic resonance imaging (MRI) is a technique of image acceleration which takes advantage of the localization of the field of view (FOV) of coils in an array. In this letter we show that metamaterial lenses based on capacitively-loaded rings can provide higher localization of the FOV. Several lens designs are systematically analyzed in order to find the structure providing higher signal-to-noise-ratio. The magnetoinductive (MI) lens is found to be the optimum structure and an experiment is developed to show it. The ability of the fabricated MI lenses to accelerate the image is quantified by means of the parameter known in the MRI community as g-factor.

---

\*Electronic address: freire@us.es

One of the most severe limitations of metamaterials for applications is their narrow band response inherent to the resonant nature of the elements that constitute the periodic structure (see [1] and references therein). In Magnetic Resonance Imaging (MRI), MR images are acquired by measuring radiofrequency (RF) magnetic fields in the MHz range inside a relatively narrow bandwidth of a few tens of kilohertz. Therefore, the narrow band response of metamaterials is not a problem for MRI, so that MRI should be then considered one of the most promising field of applications for metamaterials. In addition, since the wavelength associated with RF fields is of the order of the meters, it is possible to use conventional printed circuit techniques to develop quasi-continuous metamaterials with constituent elements and periodicities two orders of magnitude smaller than the wavelength. Several works have explored MRI applications of metamaterials [2]–[12] by using different elements to build the periodic structure, such as swiss-rolls [2]–[5], wires [6] and capacitively-loaded rings [7]–[12]. Capacitively-loaded rings have the key advantage over swiss rolls and wires of providing three dimensional (3D) isotropy when they are arranged in a cubic lattice, which is an essential property if the device has to image 3D sources.

One of the most striking properties of metamaterials is the ability of a metamaterial slab with relative permittivity  $\varepsilon$  and relative permeability  $\mu$ , both equal to  $-1$ , to behave as a super-lens with sub-wavelength resolution [13]. In the case of MRI applications, since the frequency of operation is sufficiently low, we are in the realm of the quasi-magnetostatics, and we only need a metamaterial slab with  $\mu = -1$  to behave as a super-lens [13]. In previous works, some of the authors showed that a 3D array of capacitively-loaded rings can behave as an effective homogeneous medium with  $\mu = -1$  [7]. The authors also explored both theoretically and experimentally the ability of this structure to behave as a super-lens for MRI [8]–[11]. Thus for example, it was shown that in some circumstances, this device can enhance the sensitivity of a single MRI surface coil, as a consequence of its subwavelength focusing properties [8],[9]. As it is well known, the generation of images in MRI is based on the detection of spatial variations in the phase and frequency of the RF waves absorbed and emitted by the nuclear spins of the imaged object. These spatial variations are induced by some static magnetic field gradients and the image acquisition involves many repeated measurements and then signal processing (inverse Fourier transforming) before obtaining an image of a single slice of tissue. Actually, the long acquisition time is the main drawback of MRI in comparison with computerized tomography, and time reduction without degrading

the signal-to-noise ratio (SNR) is the main aim of research in the MRI community. Image acceleration in MRI is achieved by means of techniques known in general as parallel MRI (pMRI) [15–17]. pMRI works by taking advantage of the spatially sensitive information inherent in a receiving array of multiple surface coils in order to partially replace time-consuming spatial encoding. PILS, SENSE and GRAPPA are examples of these parallel techniques [15–17]. For instance, in the PILS technique [15], it is assumed that each individual coil in the array has a localized sensitivity pattern or field of view (FOV). However, this localization takes place only at distances very close to the array because of the spreading of the magnetic field at farther distances. SENSE and GRAPPA are the commercially available techniques [16, 17]. These techniques are not restricted to linear coil configurations or localized sensitivities. However, coil sensitivity variation in the phase-encoding direction in which the reduction is performed must be ensured. In general, the ratio between the SNR in the accelerated image after parallel imaging reconstruction ( $\text{SNR}_{\text{acce}}$ ) and the SNR of a full or conventional acquisition ( $\text{SNR}_{\text{full}}$ ) decreases with the square root of the reduction or acceleration factor  $R$  (for example,  $R = 2$  means that the acquisition time reduces to one half) as well as an additional coil geometry dependent factor known as geometry g-factor in the parallel imaging community [16, 22]:

$$\frac{\text{SNR}_{\text{full}}}{\text{SNR}_{\text{acce}}} = g \cdot \sqrt{R} \quad (1)$$

The g-factor results in a spatially variant noise enhancement that strongly depends on the encoding capability of the receiver array. It is worth to mention for the discussion, that overlapping of the FOVs of adjacent coils in the array degrades the SNR of the image in the overlapping region due to the noise correlation between the coils [17]. This overlapping can be quantitatively estimated by means of the g-factor. A smart design of the array can minimize the g-factor in the overlapping region, which means that the image can be accelerated (higher  $R$ ) without degrading much the SNR. Localizing the FOV results in a reduction of the g-factor, and therefore, the image can be accelerated without degrading the SNR.

In a previous work, the authors suggested that a metamaterial super-lens can provide a time reduction in the acquisition process if the imaging ability of this device is combined with the encoding process of parallel techniques [14]. This suggestion was numerically [9] and experimentally [10] investigated by the authors. The authors experimentally shown [10] that

a  $\mu = -1$  slab consisting of a 3D array of capacitively-loaded rings can help to discriminate the fields produced by the coils at deeper distances inside the patient body, so that this device could be advantageously used in pMRI techniques in order to obtain a better localization of the FOV. Although the reported device [10] actually improved the localization of the FOV, the authors also realized that the SNR was degraded in the full FOV by the presence of the lens due to the additional ohmic losses of the device [10]. Therefore, in order to achieve a practical application in pMRI, further research aimed to a reduction of these losses was required. In the present work, capacitively-loaded ring lenses with different structures have been investigated in order to look for a device providing higher SNR. This research is carried out by means of a computational tool developed by the authors for the calculation of the SNR provided by MRI coils in the presence of capacitively-loaded ring structures and a conducting phantom resembling human tissue [11]. This computational tool was previously checked by the authors with experimental results [11]. Using this method, several structures have been numerically and experimentally analyzed and an optimum structure has been found. An MR experiment is shown to prove that this optimum structure can provide image acceleration without degrading the SNR, so that it would be suitable for a practical application.

The configuration under analysis is shown in Fig.1. It consists of a two-channel array of squared coils with a metamaterial structure placed between these coils and the phantom. In a previous work [10], a similar configuration was analyzed. In this configuration the metamaterial lens had a larger area than the array. In the present research, we have found that the noise coming from the metamaterial structure is reduced significantly if the metamaterial lens is divided into two smaller lenses, each one of them with an area smaller than the area of each coil (see Fig. 1). The magnetic field produced by a coil has a central main lobe and side lobes (see Fig. 2), with side lobes corresponding to the magnetic field vortex around the conducting loop. If the magnetic field produced by the coil is decomposed into spatial Fourier harmonics, the main lobe will be represented by low harmonics whereas the side lobes will be represented by high harmonics, corresponding to the strong spatial variations of the field. The transfer function of split-ring metamaterial lenses [7, 18] has a cutoff wavenumber which prevents transferring of high harmonics, so that side lobes are not transferred by the lens. Moreover, high harmonics related with side lobes account for high losses in the lens, thus increasing noise. Therefore, it is convenient to make the area of the

lens smaller than the area of the coil in order to reduce such noise. Moreover, since the side lobes are the dominant source of the noise correlation [22] between adjacent coils in an array, it is also convenient for pMRI applications to transfer only the main lobes. When the lenses are present they transfer the main lobe but not the side lobes, so that the side lobes attenuate in air and do not reach the phantom. In absence of the lenses, the coils are closer to the phantom and the side lobes penetrate it. The distance between the coils, the lenses and the phantom can be optimized using the previously reported method [11] in order to get higher SNR. In our analysis,  $\mu = -1$  lenses corresponding to 3D arrays of two and one unit cells in depth were studied. A second type of lens proposed in the past by the authors [14, 19, 20] and termed magnetoinductive (MI) lens was also studied. The MI lens consists of a pair of parallel 2D arrays of rings. The principle of operation of the MI lens is different from the  $\mu = -1$  lens. In the MI lens, the operating frequency does not correspond to an effective value of permeability but to the frequency between two resonances [20] which are similar to plasmons in negative permittivity devices [13]. Moreover, whereas the  $\mu = -1$  lens is isotropic, the MI lens is anisotropic since it only interacts with fields which are perpendicular to the arrays. This is not a problem since the field produced by MRI coils at closer distances is mainly axial. In our analysis, it was found that the MI lens provides the higher SNR due to the lower ohmic losses introduced by the structure.

Fig. 3 shows the computation of the resistance in a squared coil of 12 cm in length in the presence of different lenses: a  $\mu = -1$  lens with two unit cells in depth, a  $\mu = -1$  lens with one unit cells in depth and a MI lens. All these lenses are 90 mm in length with  $6 \times 6$  unit cells and periodicity 1.5 cm. Dimensions of the rings are the same as in a previously reported device [8], i.e., the rings are 4.935 mm in radius and have 2.17 mm of strip width. The two arrays in the MI lens are separated by a distance of 11 mm. The results in Fig. 3.a show that the MI lens provides the lower resistance at the frequency of 63.6 MHz corresponding to the operating frequency of a 1.5T MRI system. Fig. 3.b checks this results by comparing the theoretical prediction for the MI lens with measurements carried out with an Agilent PNA series E8363B Automatic Vector Network Analyzer. Finally, Fig. 3.c shows the computation of the axial profile of the SNR provided by all these lenses, the MI lens being the structure providing the highest values at all distances.

Thus, two MI-lenses with  $6 \times 6$  rings were designed and fabricated to operate at 63.63 MHz for experiments in a 1.5 T clinical MRI scanner. Each ring is 4.935 mm in radius

and have 2.17 mm of strip width and contains a 470 pF non-magnetic capacitor. The two arrays in the MI lens are separated by a distance of 11 mm, and the distance between the coils and the lenses and between the lenses and the phantom was 6 mm. Two receive-only arrays with two  $12 \times 12$  cm<sup>2</sup> elements were built. One array has been combined with the MI-lenses. The elements in both arrays are decoupled using a shared conductor with a decoupling capacitor. Each element in both configurations was tuned to 63.63 MHz and matched to  $50 \Omega$  in presence of an agar-phantom ( $\epsilon=90$  and  $\sigma=1.2$  S/m). The elements in the arrays were also actively decoupled by a tuned trap circuit including a PIN diode in transmission. The isolation achieved between the elements in both setups was better than -30 dB. The active decoupling by the traps has been found to be better than -30 dB. In order to investigate the SNR performance of the arrays, quantitative SNR maps were calculated from a series of identical phantom images [21] for both setups using a gradient-echo sequence (parameters: TR= 500 ms, TE= 10 ms, FOV: 380 x 380 mm<sup>2</sup>, matrix: 256 x 256, slice thickness= 5 mm). All MR images were acquired in the 1.5 T whole body system (Symphony Magnetom, Siemens, Germany) sited at the University Hospital Virgen Macarena (Seville, Spain). Figure 4.a shows a comparison of the calculated SNR-maps. In the presence of the MI lenses, the distance between the coils and the phantom is 23 mm (the thickness of the lens is 11 mm), the main lobes are transferred but not the side lobes, so that the side lobes attenuate in air and do not reach the phantom. In absence of the lenses, the coils are at 6 mm from the phantom and the side lobes penetrate it. The results if Fig. 4.a make apparent the ability of the MI lenses to localize the FOV of the coils in the array. Moreover, for short distances, the SNR provided by the lenses is even higher than in absence of the lenses. This is a clear improvement in comparison with the experimental results previously reported by the authors for a lens larger than the array [10]. In addition, in order to investigate the parallel imaging capabilities of the MI lenses, GRAPPA reconstructions have been carried out [17]. Corresponding GRAPPA g-factor maps [22] and the noise correlations were calculated for a reduction factor  $R = 3$ . Figure 4.b shows a comparison of the GRAPPA g-factor maps. The g-factor obtained in the space between the FOVs when the MI lenses are present is clearly lower than in absence of the lenses, so that with the MI lenses the acquisition can be accelerated without degrading the SNR in this region. Therefore, MI lenses can find a real application in MRI as devices which allows to accelerate the image acquisition, thus providing a real benefit for patients.

- 
- [1] R. Marques, F. Martin and M. Sorolla, *Metamaterials with Negative Parameters: Theory and Microwave Applications* (Wiley, Hoboken, New Jersey, 2008).
  - [2] M.C.K. Wiltshire, J.B. Pendry, I.R. Young, D.J. Larkman, D.J. Gilderdale, J.V. Hajnal, *Science*, **291**, 849 (2001).
  - [3] V.C. Behr, A. Haase, P.M. Jakob, *Concepts in Magnetic Resonance Part B (Magnetic Resonance Engineering)*, **23B(1)**, 44 (2004).
  - [4] M. Allard, M.C.K. Wiltshire, J.V. Hajnal, R.M. Henkelman, *Proc. Intl. Soc. Mag. Reson. Med.* **13**, 871 (2005).
  - [5] M. Allard, R.M. Henkelman, *J. Magn. Reson.*, **182**, 200 (2006).
  - [6] X. Radu, D. Garray and C. Craeye, *Metamaterials*, **3**, 90 (2009).
  - [7] L. Jelinek, R. Marques, and M.J. Freire, *J. Appl. Phys.* **105**, 024907 (2009).
  - [8] M.J. Freire, R. Marques, and L. Jelinek, *Appl. Phys. Lett.* **93**, 231108 (2008).
  - [9] M. J. Freire, L. Jelinek, R. Marques and M. Lapine, *J. Magn. Res.* **203**, 81 (2010).
  - [10] J.M. Algarin, M.J. Freire, M.A. Lopez, M. Lapine, P.M. Jakob, V.C. Behr, and R. Marques, *Appl. Phys. Lett.* **98**, 014105 (2011).
  - [11] J.M. Algarin, M.A. Lopez, M.J. Freire, and R. Marques, *New J. Phys.* **13**, 115006 (2011).
  - [12] J.M. Algarin, M.J. Freire, M.A. Lopez, M. Lapine, P.M. Jakob, V.C. Behr, and R. Marques, *Appl. Phys. Lett.* **79**, 349 (2011).
  - [13] J. B. Pendry, *Phys. Rev. Lett.* **85**, 3966 (2000).
  - [14] M.J. Freire and R. Marques, *J. Appl. Phys.* **103**, 013115 (2008).
  - [15] M. A. Griswold, P. M. Jakob, M. Nittka, J. W. Goldfarb, and A. Haase, *Magn. Reson. Med.* **44**, 602 (2000).
  - [16] K.P. Pruessmann, M. Weiger, M.B. Scheidegger, and P. Boesiger, *Magn. Reson. Med.* **42**, 952 (1999).
  - [17] M. A. Griswold, P. M. Jakob, R. M. Heidemann, M. Nittka, V. Jellus, J. Wang, B. Kiefer, and A. Haase, *Magn. Reson. Med.* **47**, 1202 (2002).
  - [18] J.M. Algarin, M.J. Freire, and R. Marques, *Metamaterials* **5**, 107 (2011).
  - [19] M.J. Freire and R. Marques, *Appl. Phys. Lett.* **86**, 182505 (2005).
  - [20] M.J. Freire and R. Marques, *J. Appl. Phys.* **100**, 063105 (2006).

- [21] M.A. Ohliger, P. Ledden, C.A. McKenzie, and D.K. Sodickson, *Magn. Reson. Med.* **52**, 628 (2004).
- [22] F.A. Breuer, S.A.R. Kannengiesser, M. Blaimer, N. Seiberlich, P.M. Jakob, and M.A. Griswold, *Magn. Reson. Med.* **62**, 739 (2009).



## ACKNOWLEDGEMENTS

This work has been supported by the Spanish Ministerio de Ciencia e Innovacion under projects Consolider-EMET CSD2008-00066 and TEC2010-16948 (SEACAM) and by the Spanish Junta de Andalucia under project TIC-06238 (METAMED). We want also thank Dr. Carlos Caparros, from University Hospital Virgen Macarena (Seville, Spain), for his advice.

## CAPTION TO FIGURES

Figure 1. a): Sketch of a 3D  $\mu = -1$  lens with two unit cells in depth and a MI lens, both of them with an area of  $6 \times 6$  unit cells. b): Photographs of the real devices sketched in a). c): Sketch Configuration under analysis and consisting of two lenses placed between a two-channel array of coils and a phantom. d): Photograph of the real configuration with MI lenses.

Figure 2. a): Magnetic field lines of a circular coil of radius  $R$ . b): Plot of the axial field of the same coil at an axial distance of  $R$ .

Figure 3. a): Calculation of the input resistance of a coil of 12 cm in diameter at 15 mm from 3D  $\mu = -1$  lenses of two-unit cells in depth, one unit-cell in depth and a MI lens. b): Comparison between calculation and measurement for the input resistance of the MI lens.

Figure 4. (a) SNR maps and (b) g-factor maps of an agar phantom for a two-channel array of coils with and without MI lenses.

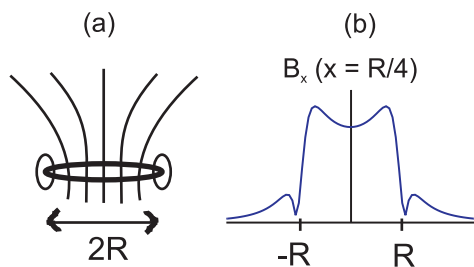


Fig.1

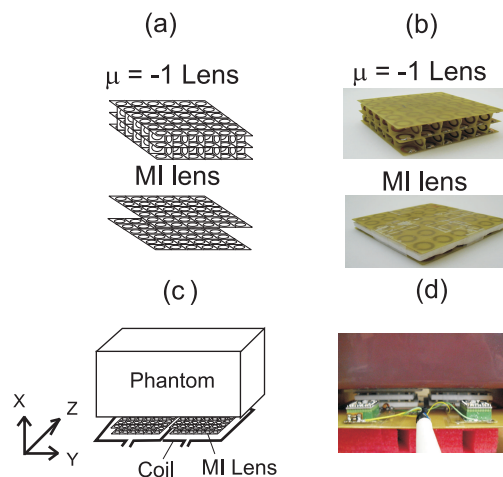


Fig.2

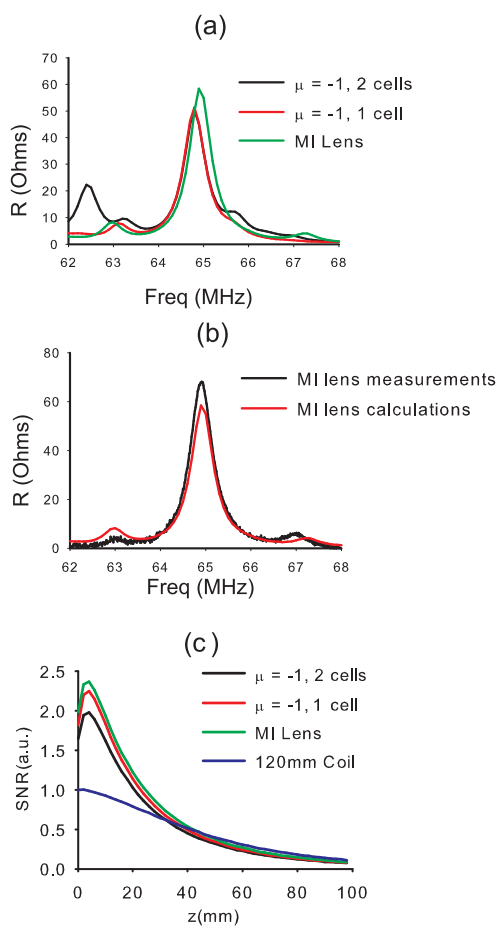


Fig.3

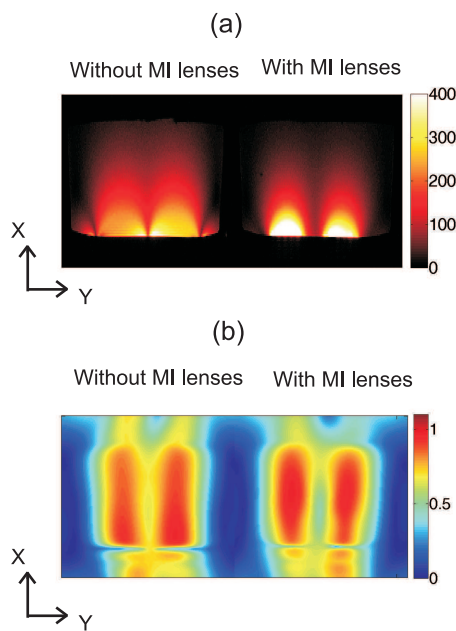


Fig.4